Mon. Not. R. Astron. Soc. **325**, 34–48 (2001)

# Chemical evolution using smooth particle hydrodynamical cosmological simulations – I. Implementation, tests and first results

M. B. Mosconi,[1] P. B. Tissera,[2,3★] D. G. Lambas[1,3] and S. A. Cora[3,4]

[1]*Grupo I.A.T.E., Observatorio Astronómico de Córdoba, Argentina*
[2]*Instituto de Astronomía y Física del Espacio, Casilla de Correos 67, Suc. 28, Buenos Aires (1428), Argentina*
[3]*Consejo Nacional de Investigaciones Científicas y Técnicas, Argentina*
[4]*Observatorio Astronómico de La Plata, U.N.L.P., Argentina*

Accepted 2000 November 8. Received 2000 October 19; in original form 2000 February 29

**ABSTRACT**

We develop a model to implement metal enrichment in a cosmological context based on the hydrodynamical code AP3MSPH described by Tissera, Lambas and Abadi. The star formation model is based on the Schmidt law, and has been modified in order to describe the transformation of gas into stars in more detail. The enrichment of the interstellar medium resulting from Type I and II supernovae explosions is taken into account by assuming a Salpeter initial mass function and different nucleosynthesis models. The various chemical elements are mixed within the gaseous medium according to the smooth particle hydrodynamics technique. Gas particles can be enriched by different neighbouring particles at the same time. We present tests of the code that assess the effects of resolution and model parameters on the results. We show that the main effect of low numerical resolution is to produce a more effective mixing of elements, resulting in abundance relations with less dispersion. We have performed cosmological simulations in a standard cold dark matter scenario, and we present results of the analysis of the star formation and chemical properties of the interstellar medium and stellar population of the simulated galactic objects. We show that these systems reproduce the abundance ratios for primary and secondary elements of the interstellar medium, and the correlation between the (O/H) abundance and the gas fraction of galaxies. We find that the star formation efficiency, the relative rate of Type II supernovae to Type I supernovae and the lifetime of binary systems, as well as the stellar nucleosynthesis model adopted, affect the chemical properties of baryons. We have compared the results of the simulations with an implementation of the one-zone simple model, finding significant differences in the global metallicities of the stars and gas as well as their correlations with dynamical parameters of the systems. The numerical simulations performed provide a detailed description of the chemical properties of galactic objects formed in hierarchical clustering scenarios and prove to be useful tools to deepen our understanding of galaxy formation and evolution.

**Key words:** hydrodynamics – methods: numerical – galaxies: abundances – galaxies: evolution – galaxies: formation – cosmology: theory.

## 1 INTRODUCTION

In recent years, our knowledge of the high-redshift Universe has increased dramatically, allowing us to start constructing a picture of how the different morphological types evolve (e.g. Steidel & Hamilton 1992; Madau 1995; Lilly et al. 1995; Cowie et al. 1996; Ellis et al. 1996; Steidel et al. 1998). In particular, the comoving star formation history first depicted by Madau et al. (1996) has resulted in a very useful way of quantifying galaxy evolution, under certain hypotheses. Since star formation directly translates into metal enrichment of the interstellar medium (ISM), observations of these two processes help astronomers to constrain models of the formation of the structure. In particular, Lyman alpha forests, damped Lyman alpha systems and Lyman alpha break galaxies have all contributed to the estimation of the cosmic metal ejection and star formation rates (e.g. Lu et al. 1996; Pettini et al. 1997). However, we are still far from drawing a consistent picture, since several points remain to be clarified. In this respect, the

★ E-mail: patricia@iafe.uba.ar

integration of the dust-corrected cosmic star formation history of the Universe up to $z = 0$ can account for the entire stellar mass content in spirals and spheroids at present times. However, when we look at the metal content at $z \simeq 2.5$, only 10 per cent of what is expected is actually measured (Renzini 1998). Regarding the chemical properties of galaxies, most of the available observations are restricted to the Galaxy, and in particular to the solar neighbourhood (e.g. Edvardsson et al. 1993; Gratton et al. 1996; Rocha-Pinto, Maciel & Flynn 2000). Extragalactic observations of H II regions provide information on the chemical content in other galaxies (e.g. Pagel 1992; Garnett et al. 1995; Kennicutt & Garnett 1996; Kobulnicky & Skillman 1996).

Chemical evolution models are a useful tool to attempt to study the physical processes that might determine the chemical characteristics of different galaxies. Detailed modelling can be found in studies of the Galaxy (e.g. Ferrini et al. 1992; Tosi 1996; Chiappini, Matteucci & Gratton 1997, and references therein). These analytical models treat stellar evolution carefully. However, they cannot account for dynamical evolution, and certainly not for hierarchical clustering. From a numerical point of view, metallicity enrichment mechanisms have been implemented in hydrodynamical simulations in different ways. The first attempts were done by Larson (1975, 1976). Other implementations came after using diverse techniques such as chemodynamical models (e.g. Burkert, Truran & Hensler 1992; Samland, Hensler & Theis 1997), which describe in more detail the interstellar medium evolution. On the other hand, this approach uses a very simple prescription for galaxy formation where the dark matter halo is either not considered at all or assumed to be static. However, there is strong evidence from observations of normal spirals that the dark matter is dynamically important within the luminous radius (e.g. Bottema 1992; Courteau, de Jong & Broeils 1996; Rhee 1996), and that the response of the dark matter to the presence of baryons affects their evolution (Blumenthal et al. 1986; Tissera & Domínguez-Tenreiro 1998) and, as a consequence, the star formation process (Mihos & Hernquist 1996; Barnes & Hernquist 1996; Tissera 2000; Navarro & Steinmetz 2000). A first approach to include chemical evolution in a smooth particle hydrodynamical (SPH) code is described by Steinmetz & Müller (1994, 1995) followed by Raiteri, Villata & Navarro (1996). These works run prepared-cosmological initial conditions where the formation and evolution of only one object was studied. These models have shed light on some physical mechanisms that may control metallicity in galaxies, and have also shown that hierarchical clustering scenarios may form galactic objects that resemble Milky Way-type galaxies from a chemical point of view. However, the SPH models with chemical implementations hitherto published are restricted to the Galaxy. It would be very important for the study of the formation and evolution of galaxies to be able to analyse a variety of galactic objects with different evolutionary histories. Hydrodynamical cosmological simulations are more suited to tackle this problem since the non-linear evolution of the matter is naturally accounted for, and physical processes can be more consistently implemented. These models can provide coherent well-described environments for all objects and a complete record of their formation and evolution. The drawback is the treatment of numerical resolution effects.

In this paper, we concentrate on the description of the chemical model that has been implemented in a cosmological hydrodynamical AP3M code. First results on galaxy formation, global chemical properties and comparison with observations are reported. Detailed analysis of the chemical properties of the ISM and stellar population in galaxy-like objects, such as abundance gradients, age–metallicity relations, etc., are given by Tissera et al. (in preparation, hereafter Paper II).

This paper is organized as follows. Section 2 describes the star formation process and the metal enrichment implementation. In Section 3 we assess the performance of the chemical model. In Section 4 we present the first results on galaxy formation and chemical evolution. Section 5 summarizes the results.

## 2 NUMERICAL MODEL

We use a cosmological numerical code based on the SPH technique described by Tissera, Lambas & Abadi (1997). The SPH algorithm has been coupled to the AP3M gravitational code (Thomas & Couchman 1992), in order to follow the gravitational and hydrodynamical evolution of particles within a cosmological context. For the sake of simplicity, and as a first step in the development of this chemical cosmological code, simulations have been run considering that the gas cools down by using the approximation given by Dalgarno & McCray (1972).

### 2.1 Star formation

In general, the modelling of star formation (SF) in SPH simulations is based on the Schmidt law and a series of hypotheses to select suitable SF regions. However, how it is actually implemented within each particular code depends on the different authors (e.g. Katz 1992; Navarro & White 1994; Tissera et al. 1997). In this paper, we describe a modified version of the SF implemented by Tissera et al. (1997) in order to be able to track the transformation of gas into stars in more detail, within a given gas particle.

We include the SF algorithm as follows. Gas particles are eligible to form stars if they are cold ($T < T_*$) and satisfy a density criterion: $\rho_{\rm gas} > \rho_{\rm crit}$. This density criterion arises by requiring the cooling time of a gas particle to be smaller than its dynamical time. The critical temperature $T_*$ is taken as the minimum value provided by the cooling functions ($T_* \sim 10^4$ K). Finally, gas particles have to be part of a collapsing region. This requirement is imposed by selecting particles in a convergent flow ($\nabla \cdot \boldsymbol{v} < 0$). When a gas particle satisfies all these conditions, star formation occurs according to the Schmidt law,

$$\frac{{\rm d}\rho_{\rm star}}{{\rm d}t} = c\frac{\rho_{\rm gas}}{t_*}, \tag{1}$$

where $c$ is the star formation efficiency and $t_*$ is a characteristic time-scale assumed to be proportional to the dynamical time of the particle [$t_* = t_{\rm dyn} = (3\pi/16G\rho_{\rm gas})^{1/2}$]. Then, each stellar mass formed in a particle at a certain SF episode is given by $\Delta_{\rm star} = C\rho_{\rm gas}^{3/2}\Delta t$, where $\Delta t$ is the time-step of integration ($\Delta t = 1.3 \times 10^7$ yr) and $C$ is a new SF efficiency. Note that, according to equation (1), in order to go from density to mass, the volume of the new-born stars has to be assumed. Taking into account that the process we are modelling happens *within a gas particle* and that, according to observations, SF occurs normally in clusters, not in isolation, we assume that the volume occupied by the fraction of new-born stars is constant for all them. Thus, it can be absorbed in the new constant, $C$.

According to this SF scheme, in a given baryonic particle there could be several SF episodes that had occurred at different times. The gaseous mass of the baryonic particle is reduced by $\Delta_{\rm star}$ until

its gas reservoir is depleted. A minimum gas mass equal to 5 per cent of the initial gas mass component is left over in each particle. When a particle reaches this minimum mass, it is transformed completely into a star particle and hereafter behaves as collisionless matter. Each $\Delta_{\rm star}$ formed can be followed up in time. The number of stars of a given mass within $\Delta_{\rm star}$ is estimated by assuming an initial mass function (IMF). Hence, a baryonic particle may be formed by gaseous and stellar components in different proportions according to its history of evolution (hereafter, hybrid particle). The stellar component can be made up of different stellar populations with different ages and chemical properties, which have been formed at different SF episodes. The chemical properties of each stellar population ($\Delta_{\rm star}$) reflect the chemical state of the ISM at the time of its formation.

The decoupling between gas and stars depends on the actual rate at which stars are formed in each baryonic particle, which, in turn, depends on each evolutionary path. Hybrid particles may introduce some numerical artefacts since the stellar populations follow the gas evolution when they should probably not. However, this is not a trivial problem that can be easily resolved. Work to improve the decoupling process is under way and will be presented in a separate paper.

### 2.2 Metal production

Metals are produced and ejected into the interstellar medium at the end of the life of stars. Most chemical elements are ejected by Type II supernovae (SNII), except for iron, which is mainly produced by Type I supernovae (SNI). Particles are assumed to be initially formed by hydrogen and helium in primordial abundances (H = 0.75, He = 0.25). The first generations of stars with primordial abundances immediately enrich the ISM from which the new generations are born. It has to be stressed that we are not including the effects of (thermal or kinetic) energy injection into the ISM due to SN explosions. For the sake of simplicity we have split the treatment of the feedback problem into two stages. First, we include chemical enrichment (this paper), and in a second step, we intend to develop an energy feedback model. There have been several attempts to implement energy feedback in SPH codes by injecting either thermal (e.g. Katz 1992) or kinetic (e.g. Navarro & White 1994; Metzler & Evrard 1994; Navarro & Steinmetz 2000; Springel 2000) energies into the gas component due to SN explosions. However, these methods are still controversial, leaving this problem as an open question for galaxy formation.

Let us now describe the nucleosynthesis prescriptions adopted in this model:

(i) *Type II supernovae.* We assume that stars more massive than $8\,{\rm M}_{\odot}$ end their lives as SNII. In order to estimate their number, we adopt a Salpeter IMF with a lower and upper mass cut-off of 0.1 and $120\,{\rm M}_{\odot}$, respectively. The IMF adopted gives the total number of SNII formed in a certain range of stellar masses in a given $\Delta_{\rm star}$ at a certain time. Supernovae are thought to eject their whole metal production within a few $10^7$ yr. In particular, we assume that their lifetime is equal to the integration time-step of the simulations.

For comparison, we resort to the metal ejecta models of both Portinari, Chiosi & Bressan (1998, hereafter PCB98) and Woosley & Weaver (1995, hereafter WW95), and follow the evolution of different elements according to the information provided by those authors. PCB98 give metal yields for stars up to $120\,{\rm M}_{\odot}$, while WW95 assume that stars larger than $40\,{\rm M}_{\odot}$ end their lives as black holes. We consider the following elements according to each author: H, $^4$He, $^{12}$C, $^{16}$O, $^{24}$Mg, $^{28}$Si, $^{56}$Fe for both PCB98 and WW95, and also $^{14}$N, $^{20}$Ne, $^{32}$S, $^{40}$Ca, $^{62}$Zn for WW95.

(ii) *Type I supernovae.* Following Matteucci & Francois (1989), we assume that Type Ia supernovae (SNIa) originate from carbon deflagration in C–O white dwarfs in binary systems. It is assumed that the masses of these binary systems are likely to be in the range $3$–$16\,{\rm M}_{\odot}$. The adopted nucleosynthesis prescriptions are taken from Thielemann, Nomoto & Hashimoto (1993). Type Ib supernovae (SNIb) are assumed to be half the total number of SNI and to produce only iron ($\approx 0.3\,{\rm M}_{\odot}$ per explosion).

The main interest in including SNI events in the models is that they contribute with a substantial amount of iron. This element is fundamental to attempt to reproduce several observational results (see also Chiappini et al. 1997). The relative rate of SNI to SNII explosions has been observationally estimated in the solar neighbourhood and from extragalactic sources (van der Bergh 1991). These estimations suggest a range of possible values for the total SNI rate (SNRI) with respect to that of SNII (SNRII) of $2 \leqslant {\rm SNRII/SNRI} \leqslant 3.11$.

Binary systems evolve for a certain period of time ($t_{\rm SNI}$) during which mass is transferred from the secondary to the primary star until the Chandrasekhar mass is exceeded and an explosion is triggered. It is generally assumed that a fair fraction of SNI will explode after a period of $t_{\rm SNI} \approx 10^8$–$10^9$ yr (Greggio 1996). It is straightforward to estimate when SNI will explode and eject metals into the neighbouring region, since the formation time of each $\Delta_{\rm star}$, in a given baryonic particle, is known. The effects of varying both the SNRII/SNRI relative rate (hereafter, $\Theta_{\rm SN}$) and $t_{\rm SNI}$ are analysed and the results are confronted with observations in the following sections.

To sum up, the free parameters of our chemical model are: the star formation efficiency ($C$), the initial mass function (IMF), its upper and lower mass cut-offs, the relative rate of different types of supernovae ($\Theta_{\rm SN}$), the lifetime of binary systems that end as SNI ($t_{\rm SNI}$) and the yields. Regarding the IMF, we are going to adopt a constant and unique one throughout this paper.

### 2.3 Model for metal ejection

How the chemical elements are distributed and mixed in the interstellar medium is a complex problem which is far from being solved from a theoretical point of view (e.g. Tenorio-Tagle et al. 1999). Furthermore, numerical simulations do not reach enough resolution to treat properly this small-scale mixing process together with the process of galaxy assembly. Hence, the ejection and mixing of elements have to be modelled in a heuristic way.

We use the SPH technique to distribute the metals within the neighbouring sphere of the $j$ particle where a $\Delta_{\rm star}$ is formed. According to this technique, the value of a certain parameter at the location of the $j$ particle can be estimated by using the information stored in its neighbourhood, which is determined by the $i$ neighbouring particles within its smoothing length ($h_j$).

Using this concept, we can define the total mass ($M_j^k$) of a given chemical element $k$ ejected by a $j$ particle due to SNI or SNII, as

$$M_j^k = \sum_{i=1}^{n_{\rm v}} m_i/\rho_i M_j^k W(r_i - r_j, h_{ij}), \qquad (2)$$

where $n_{\rm v}$ is the number of $i$ neighbours of the $j$ particle ($n_{\rm v} \approx 40$), $m_i$ and $\rho_i$ are the gas mass and density of the $i$ particle, respectively, and $W(r_i - r_j, h_{ij})$ and $h_{ij}$ are the symmetrized kernel

and smoothing length, respectively. In this scheme, each $i$ neighbouring particle gets a contribution of each metal defined by

$$M_i^k = m_i/\rho_i M_j^k W(r_i - r_j, h_{ij}). \quad (3)$$

The $j$ particle where the stellar mass has just formed is also included in this process. The masses of H and He are proportionally decreased according to the metal mass received by each particle, so that its total mass is always conserved.

The distribution of metals by using the SPH technique allows metals to spread out and enrich gas particles that may have not experienced SF but are close enough to other SF regions, working as an effective mixing mechanism. Note that gas particles can be enriched by more than one neighbour at each time-step. It has to be mentioned that numerical resolution would affect the mixing of metals since it also affects the determination of the neighbours. In Section 3, we will discuss this point in more detail. In the present implementation, metal mixing occurs only tied to the SF process, in the sense that only new-born elements are distributed.

One advantage of this implementation is that particles move according to the equations of gravitation and hydrodynamics, leaving behind the closed-box hypothesis, among others. Particles with different astrophysical and chemical properties are mixed, particularly during violent events such as interaction and mergers, so that reproducing observations becomes a more challenging task.

## 3 TESTS

We carry out a series of simple tests to assess the effects of both numerical resolution and the variation of the different parameters ($C$, $\Theta_{\rm SN}$, $t_{\rm SNI}$) on the chemical properties of baryons. We also intend to evaluate the dependence of the results on the two adopted nucleosynthesis models, PCB98 and WW95. For this purpose, we follow the evolution of a homogeneous gaseous sphere. The sphere is represented by $10^3$ gas particles initially distributed following a density profile $\rho \propto r^{-2}$, in a radius of 625 kpc, without a dark matter halo. This simple experiment gives a clear idea of how each parameter affects the chemical properties of baryons and has the advantage of a low computational cost.

### 3.1 Effects of numerical resolution

Numerical problems may affect both the process of star formation and especially the distribution of metals. With respect to the former, if dark matter haloes in galactic objects are numerically well resolved, the star formation process may not be strongly affected by the numerical resolution (see discussion in Domínguez-Tenreiro, Tissera & Sáiz 1998). This is due to the fact that dark matter determines the potential well on to which the gas settles. If dark matter haloes are well resolved, baryons are forced to distribute adequately. In this way, the gas density profiles are well reproduced and the SF can be correctly followed (Tissera 2000). Nevertheless, the gas component has to be resolved, at least, by a few hundred particles (Navarro & White 1994). In our simulations, baryonic and dark matter components are represented by particles of equal mass. Therefore, dark matter haloes are resolved by a much larger number of particles than the baryonic component. Hence, the potential wells of the larger galactic haloes are very well defined (see Tissera & Domínguez-Tenreiro 1998). Consequently, we restrict our global analysis to galactic objects resolved with more than 250 baryonic particles.

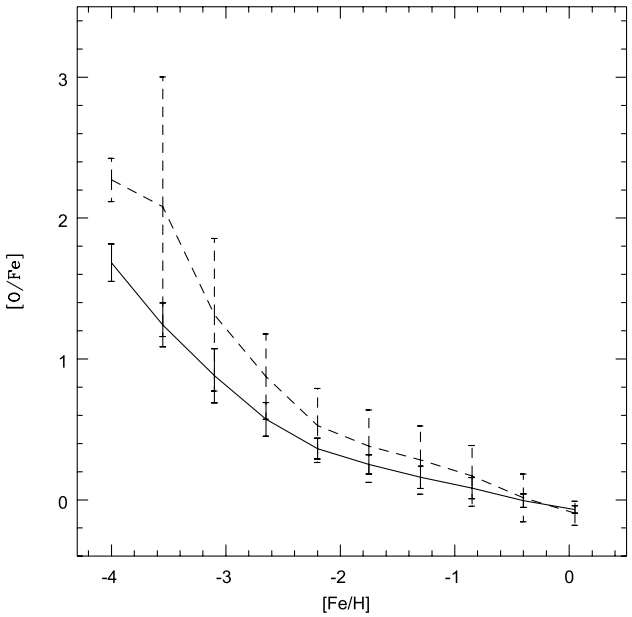


**Figure 1.** Comparison of the [O/Fe] versus [Fe/H] relation obtained from the low-resolution (solid line) and high-resolution tests (dashed lines).

On the other hand, the radius of the neighbouring sphere in which the metals produced by the stellar component are distributed is affected by the numerical resolution of the experiment. Consequently, this problem may have a non-negligible effect on the metal distribution and the chemical properties of gas and stars, and requires a more detailed analysis. For this purpose, we have studied the evolution of two gaseous spheres without dark matter haloes. Each of them represents a system with total gaseous mass of $1.3 \times 10^{11}\,{\rm M}_\odot$ and initial radius of 615 kpc. One of the experiments (E1) resolves the sphere with $10^3$ particles ($m_{\rm p} = 1.3 \times 10^8\,{\rm M}_\odot$), while the second experiment (E1H) has higher numerical resolution: $8 \times 10^3$ gas particles ($m_{\rm p} = 1.7 \times 10^7\,{\rm M}_\odot$). Since these spheres have no dark matter haloes, taking into account the former discussion, it is reasonable to expect that their star formation histories will be different. In fact, the sphere in E1H starts forming stars before its counterpart in E1. However, the effects that this earlier SF has on their metallicity is not dramatic, as can be observed from Fig. 1, where we have plotted the mean values of [O/Fe] versus [Fe/H] for both experiments. The greatest differences are obtained for the low-metallicity stars ([Fe/H] $< -3$) due to the fact that star formation begins earlier in E1H and has a greater intensity than SF in E1. As stars with higher metallicities are formed, this difference diminishes. Note that error bars in E1H comprise the distribution of E1 for [Fe/H] $> -4$ (except for the first point).

The main difference observed between these two experiments is that low numerical resolution produces a reduction in the dispersion of the distribution, as can be seen from the error bars in Fig. 1. This fact can be understood by considering that, in the experiment with lower resolution, the neighbouring sphere ($n_{\rm v} \sim 40$) comprises a larger volume, thus producing a more effective mixing of the metals in the gas. Conversely, when numerical resolution is increased, the new elements produced by a certain particle are distributed in a smaller volume. This leads to a less efficient mixing at the scale of the system, producing an increase in the metallicity dispersion. We cannot theoretically assess to what extent this dispersion has any physical meaning

since the mixing mechanisms in galaxies are not yet well understood. It might be possible that SN explosions spread metals in larger volumes than that provided by the SPH technique. This fact would produce more uniform metal distributions in the interstellar medium, as actually occurs in the low numerical resolution run.

Taking into account these experiments, we conclude that the main effect of using the SPH technique to distribute metals is that the better resolved objects (i.e. those with higher number of baryonic particles, which, in our simulations, implies larger masses) would have a larger dispersion in their chemical properties than the smaller ones. Mean values of the quantities will be considered as adequate estimations.

**Table 1.** Test: main parameters.

| S | $C$ | $\Theta_{SN}$ | $t_{SNI}$ | Yields |
|---|---|---|---|---|
| E1 | 5E−6 | 2 | 1 | WW95 |
| E2 | 5E−6 | 2 | 4 | WW95 |
| E3 | 5E−6 | 2 | 10 | WW95 |
| E4 | 5E−6 | 4 | 1 | WW95 |
| E5 | 5E−2 | 2 | 1 | WW95 |
| E6 | 5E−6 | 2 | 1 | PCB98 |

Units: $[t_{SNI}] = 10^8$ yr; $[C] = \mathrm{Mpc}^{9/2}$ $\mathrm{M}_\odot^{-1/2}\,\mathrm{yr}^{-1}$.

### 3.2 Effects of the variation of the star formation parameters

We are now going to analyse the effects that the different chemical model parameters have on the properties of the stellar populations of the spheres.

As can be seen from Table 1, experiments E1, E2 and E3 differ among each other in the lifetime of binary systems that end up as SNI. The values considered are $10^8$, $4\times10^8$ and $10^9$ yr, respectively. The SF efficiency and $\Theta_{SN}$ used are the same in these three experiments. The ratio [O/Fe] versus [Fe/H] clearly illustrates the effects of varying the parameters. Fig. 2 shows [O/Fe] versus [Fe/H] for these three experiments at different stages of evolution. As can be seen from this figure, as soon as the first stars are formed, the differences among them are very important. The smaller $t_{SNI}$ used in E1 allows a rapid production of Fe and, consequently, the number of low-metallicity stars ([Fe/H] $< -3$) is considerably lower than in E2 and E3, for all times. The larger

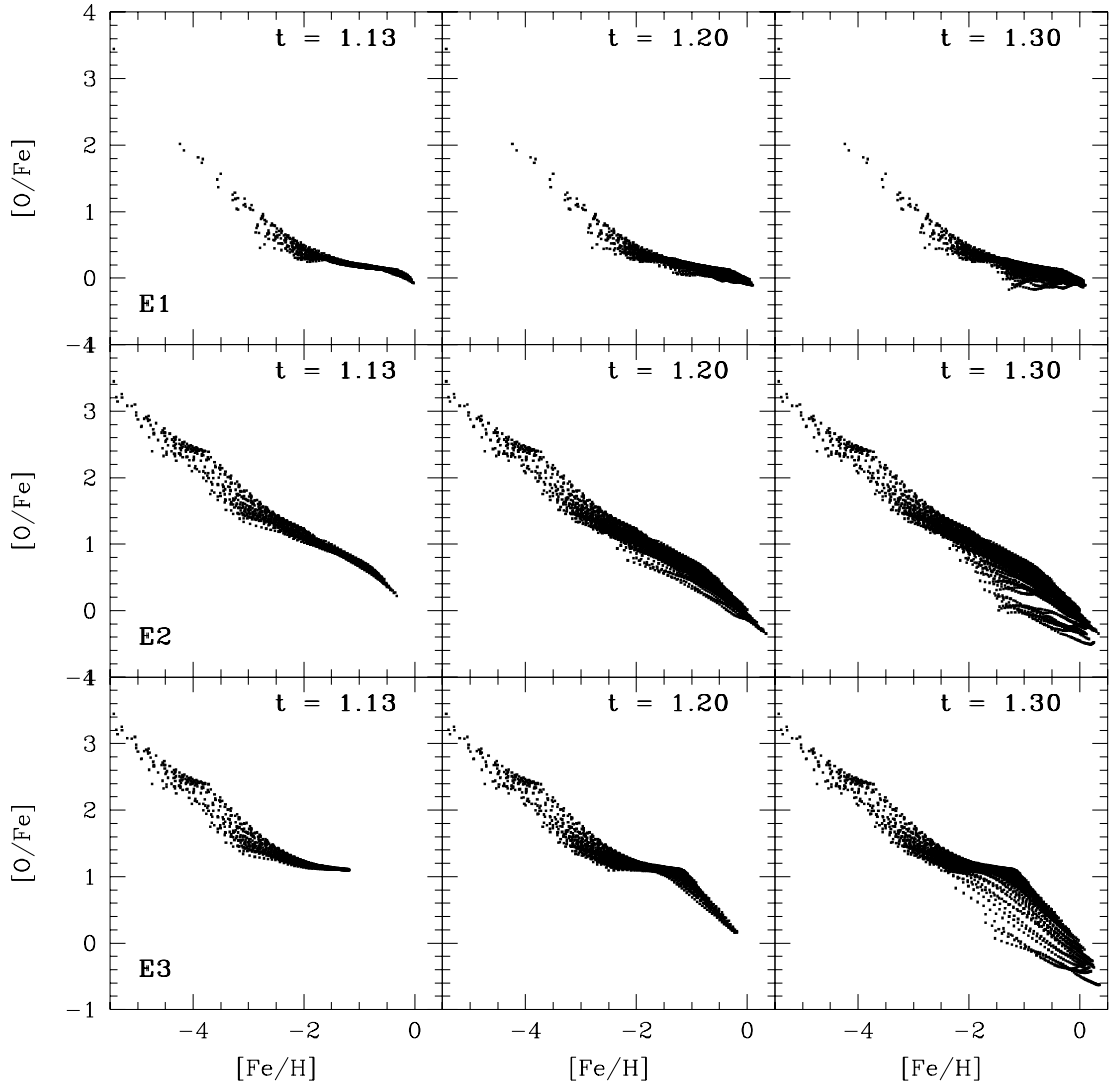


**Figure 2.** [O/Fe] versus [Fe/H] for experiments E1, E2 and E3 where the lifetime of binary systems has been varied: $10^8$ yr, $4\times10^8$ yr and $10^9$ yr, respectively. Time $t$ is given in units of $10^{10}$ yr.

$t_{SNI}$ value adopted in E3 produces a dex difference in the ratio [O/Fe] compared to the values in E1 and E2 for $t = 1.13 \times 10^{10}$ yr. As time goes on, all experiments reach solar values, although, the variation of $t_{SNI}$ among them leads to appreciably different evolutionary paths. For E1 and E2, the [O/Fe] is above observed values for the solar neighbourhood, and the steepness of the relation is much more abrupt for [Fe/H] $> -1$. Experiment E1 ($t_{SNI} = 10^8$ yr) gives a more consistent relation for stars with [O/Fe] $< 1$. In this case, the final shape and range of abundance values are set as soon as the first stars formed, which implies that, even at the early stages of evolution, this combination of SN parameters can produce stellar populations with metal contents up to solar.

In Fig. 3, we show the same relations for experiments E4, E5 and E6. In E4 we have changed the relative ratio $\Theta_{SN}$ from 2 (in E1) to 4. Since SNRII is the fraction of stars with masses greater than $8\,M_\odot$ in a certain time-step, given by the IMF adopted, an increase in the ratio $\Theta_{SN}$ implies a decrease of SNRI. The effect of the variation of this parameter gives the expected differences in the abundance tracks. Note that there is no change in the slope of the [O/Fe] versus [Fe/H] relation, but the abundances in E4 do not get to solar values because there are not enough SNI to produce the necessary amount of Fe.

In experiment E5 we use a higher SF efficiency than that in E1. In this case, stars are formed faster and the gas is enriched very efficiently so that the new-born stars immediately evolve to higher-metallicity regions. As a consequence, the low-metallicity tail in the [O/Fe] versus [Fe/H] relation vanishes. Note that, the higher the $C$ value used, the larger the stellar masses ($\Delta_{star}$) formed, so that the number of SF events in a given baryonic particle diminishes. This is the reason why the number of points in E5 is smaller when compared to the distribution in E1. The important aspect to remark is that, in E5, the range of metallicity covered by the stellar populations is considerably smaller. This implies that a very efficient SF process can enrich the medium to solar values very quickly, so that most stars would tend to be located in the high-metallicity region.

The comparison between experiments E1 and E6 clearly illustrates how the simulation results depend on the two yield models, PCB98 and WW95. The features of the [O/Fe] versus [Fe/H] relation in E6 can be appreciated in the bottom row of Fig. 3. The main characteristic observed for this experiment,

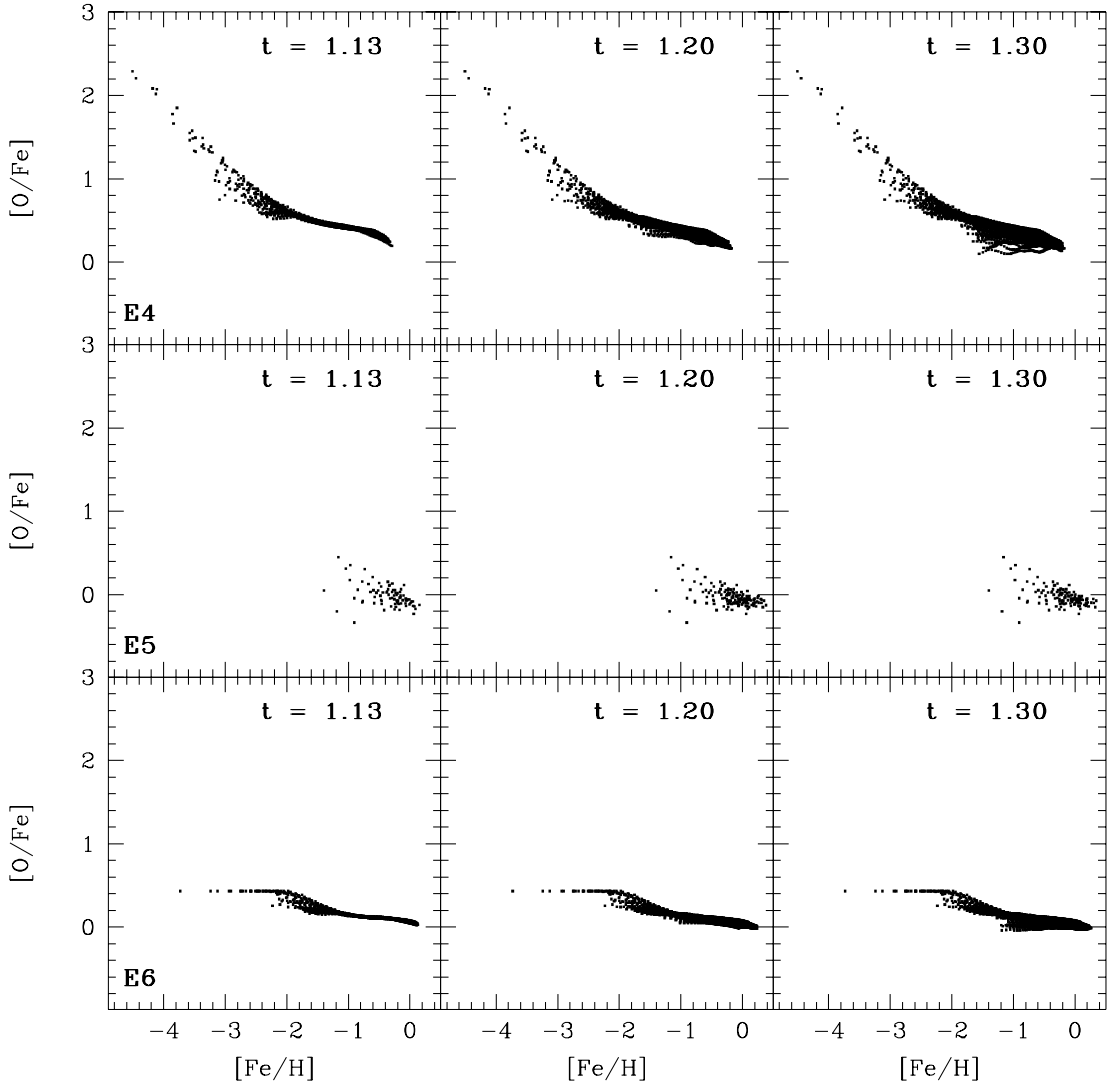


**Figure 3.** [O/Fe] versus [Fe/H] for experiments E4, E5 and E6 where the relative ratio of SNII/SNI ($\Theta_{SN}$), the star formation efficiency ($C$) and the nucleosynthesis yields have been changed with respect to E1. Time $t$ is given in units of $10^{10}$ yr.

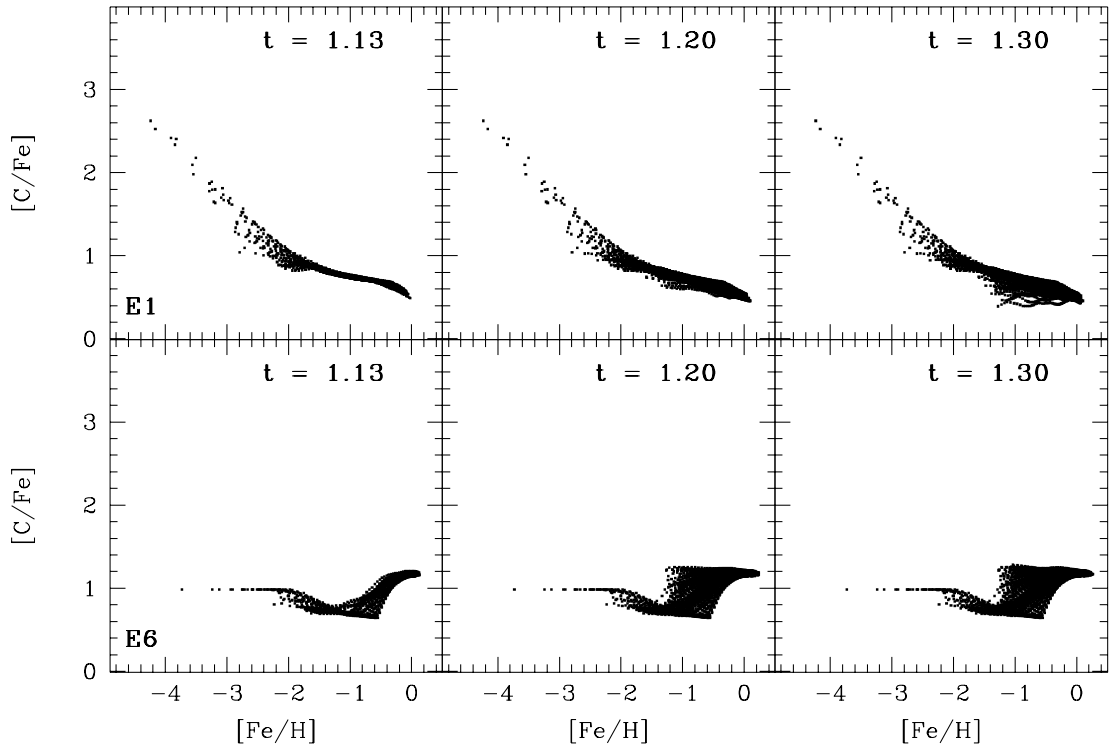


**Figure 4.** Comparison of the [C/Fe] versus [Fe/H] relation for experiments E1 (WW95 yield) and E6 (PCB98 yield). Time $t$ is given in units of $10^{10}$ yr.

where PCB98 yields were used, is the lack of the low-metallicity tail ([Fe/H] $< -3$), which can be appreciated in E1. On the other hand, the low-metallicity stars in E6 ([Fe/H] $< -2$) have almost constant values of [O/Fe], in contrast with the results of E1, where a gradient is observed. This difference arises because PCB98 yields produce more iron with respect to the other elements than WW95, up to an order of magnitude more, in some cases. So, stars are rapidly brought to lower abundance ratios with respect to iron. Despite this fact, these relations are quite similar, with the exception that WW95 seems to reach slightly higher metallicity values for the same model parameters at $z = 0$. This fact implies that PCB98 yields for enriched stars produce, in general, more elements than those of WW95. The comparison of other chemical elements shows that the major difference is in the [C/Fe] versus [Fe/H] relation. In Fig. 4, we show this relation for experiments E1 and E6 as a function of time. As clearly seen in the case of E6, there is an excess of carbon in relation to iron for [Fe/H] $> -1.2$ which produces a positive gradient.

To sum up, we find that all SF and SN parameters have non-negligible effects on the chemical properties of baryons. Then, in order to choose the correct combination of SN and SF parameters, a detailed comparison with observations has to be done.

## 4 GALAXY FORMATION

We are now interested in applying this model to the study of galaxy formation in a cosmological framework. As a first step, we look at the global properties of galaxy-like objects (GLOs) and compare them with observations. The different formation and evolutionary histories of each GLO (i.e. collapse time, merger tree, properties of progenitors, interactions, etc.) may affect their SF and chemical content in a complex way, so that, even in the same experiments, GLOs may exhibit different characteristics.

**Table 2.** Cosmological simulations.

| S | $C$ | $\Theta_{SN}$ | $t_{SNI}$ | Yields |
|---|---|---|---|---|
| S1 | 5E−6 | 2 | 1 | PCB98 |
| S2 | 5E−6 | 2 | 1 | WW95 |
| S3 | 5E−4 | 2 | 1 | WW95 |
| S4 | 5E−4 | 3 | 5 | WW95 |
| S5 | 5E−5 | 2 | 1 | WW95 |
| S6 | 5E−6 | 2 | 1 | WW95 |
| S7 | 5E−6 | 2 | 1 | WW95 |

Units: $[t_{SNI}] = 10^8$ yr; $[C] = \mathrm{Mpc}^{9/2}\ \mathrm{M}_\odot^{-1/2}\ \mathrm{yr}^{-1}$.

This fact makes cosmological simulations a very useful tool for chemical evolution studies.

The traditional model used to study chemical evolution is the so-called one-zone simple model, based on two main assumptions: the system is isolated (i.e. no inflows or outflows) and well mixed (i.e. instantaneous recycling), at all times (van der Bergh 1962; Schmidt 1963; Tinsley 1980). Other hypotheses are related to the initial condition of the gas, the IMF and nucleosynthesis yields. We remark on the first two assumptions since they are inconsistent with the formation and evolution of galaxies in a hierarchical clustering scenario. In our experiments, structures form within a cosmological model suffering physical processes such as mergers, encounters, inflows, etc., which may affect the dynamics and kinematics of the dark matter and baryonic matter. Although some authors have included inflows and relaxed the hypothesis of instantaneous recycling (e.g. Chiappini et al. 1997), these models are not formulated in a cosmological framework and do not include dynamical effects that may affect the SF process and the mixing of chemical elements. Regarding the IMF and initial condition of the gas, we adopt a Salpeter IMF for all times, and the gas is assumed to be initially in primordial abundances.

**Table 3.** Galaxy-like objects: main parameters.

| S | GLO | $N_{dark}$ | $N_{bar}$ | $V_{vir}$ | $R_{opt}$ | $V_{opt}$ | $M_{star}$ | $Z_{gas}/Z_{\odot}$ | $Z_{star}/Z_{\odot}$ |
|---|---|---|---|---|---|---|---|---|---|
| S1 | 596 | 4049 | 542 | 137.67 | 23.68 | 224.67 | 5.45 | 0.45 | 0.46 |
| | 538 | 4574 | 576 | 143.04 | 16.46 | 203.47 | 1.83 | 0.28 | 0.45 |
| | 538b | 4655 | 588 | 143.92 | 19.16 | 186.41 | 3.46 | 0.49 | 0.45 |
| | 536 | 5036 | 636 | 147.74 | 19.89 | 243.13 | 6.25 | 0.48 | 0.47 |
| | 456 | 6297 | 931 | 160.18 | 18.09 | 261.21 | 8.07 | 0.54 | 0.39 |
| | 426 | 2433 | 343 | 116.41 | 12.36 | 200.53 | 2.60 | 0.45 | 0.44 |
| | 421 | 1848 | 267 | 106.11 | 19.61 | 166.06 | 1.43 | 0.26 | 0.31 |
| | 334 | 1848 | 267 | 106.31 | 19.61 | 166.05 | 1.43 | 0.26 | 0.31 |
| | 347 | 5752 | 724 | 154.41 | 14.06 | 246.20 | 5.46 | 0.61 | 0.45 |
| | 347b | 5727 | 726 | 154.20 | 12.22 | 196.96 | 2.56 | 0.49 | 0.51 |
| | 325 | 5385 | 699 | 151.23 | 8.28 | 280.88 | 5.25 | 0.49 | 0.36 |
| | 312 | 1858 | 271 | 106.54 | 14.08 | 190.47 | 2.12 | 0.46 | 0.46 |
| | 221 | 1991 | 285 | 108.93 | 7.63 | 208.03 | 3.14 | 0.56 | 0.47 |
| S2 | 596 | 4034 | 541 | 137.45 | 18.99 | 301.70 | 5.85 | 0.19 | 0.34 |
| | 538 | 4591 | 584 | 143.29 | 18.74 | 251.69 | 2.37 | 0.17 | 0.24 |
| | 538b | 4637 | 589 | 143.77 | 11.25 | 246.80 | 3.24 | 0.21 | 0.27 |
| | 536 | 5019 | 627 | 147.46 | 14.82 | 319.25 | 6.57 | 0.20 | 0.30 |
| | 456 | 6322 | 932 | 160.35 | 21.63 | 323.83 | 7.36 | 0.19 | 0.23 |
| | 426 | 1828 | 315 | 106.79 | 5.60 | 290.85 | 4.60 | 0.37 | 0.36 |
| | 421 | 2466 | 340 | 116.83 | 12.50 | 256.97 | 2.18 | 0.17 | 0.19 |
| | 334 | 1863 | 266 | 106.48 | 23.28 | 203.43 | 1.67 | 0.09 | 0.24 |
| | 347 | 5770 | 720 | 154.52 | 14.64 | 308.19 | 5.41 | 0.27 | 0.29 |
| | 347b | 5715 | 721 | 154.10 | 9.19 | 249.24 | 2.73 | 0.22 | 0.28 |
| | 325 | 5478 | 703 | 152.01 | 12.91 | 315.70 | 5.37 | 0.23 | 0.21 |
| | 312 | 1840 | 271 | 106.24 | 15.67 | 239.76 | 2.23 | 0.19 | 0.21 |
| | 221 | 1978 | 289 | 108.78 | 29.99 | 217.00 | 2.98 | 0.23 | 0.23 |
| S3 | 596 | 4061 | 545 | 137.80 | 18.12 | 306.16 | 6.37 | 0.39 | 0.52 |
| | 538 | 4570 | 590 | 143.16 | 9.67 | 258.72 | 3.42 | 0.59 | 0.64 |
| | 538b | 4541 | 588 | 142.85 | 22.15 | 246.53 | 2.68 | 0.20 | 0.34 |
| | 536 | 5004 | 629 | 147.40 | 17.18 | 327.41 | 7.18 | 0.20 | 0.27 |
| | 456 | 6536 | 935 | 161.95 | 15.33 | 332.28 | 10.78 | 0.25 | 0.65 |
| | 426 | 2451 | 339 | 116.56 | 7.26 | 263.70 | 2.61 | 0.48 | 0.47 |
| | 421 | 1703 | 320 | 104.72 | 4.26 | 286.90 | 5.47 | 0.38 | 0.53 |
| | 334 | 1847 | 273 | 106.00 | 18.54 | 210.09 | 2.23 | 0.17 | 0.60 |
| | 347 | 5874 | 724 | 155.37 | 38.15 | 337.76 | 9.57 | 0.16 | 0.29 |
| | 325 | 5502 | 714 | 152.32 | 9.28 | 327.38 | 5.98 | 0.26 | 0.33 |
| | 312 | 1876 | 275 | 106.89 | 13.97 | 239.87 | 2.63 | 0.17 | 0.26 |
| | 221 | 2009 | 293 | 109.32 | 7.18 | 249.48 | 2.55 | 0.21 | 0.37 |
| S4 | 596 | 4061 | 545 | 137.80 | 18.12 | 306.16 | 6.37 | 0.17 | 0.25 |
| | 538 | 4570 | 590 | 143.16 | 9.67 | 258.72 | 3.42 | 0.18 | 0.25 |
| | 538b | 4541 | 588 | 142.85 | 22.15 | 246.53 | 2.68 | 0.13 | 0.25 |
| | 536 | 5004 | 629 | 147.40 | 17.18 | 327.41 | 7.18 | 0.18 | 0.21 |
| | 456 | 6536 | 935 | 161.95 | 15.33 | 332.28 | 10.78 | 0.21 | 0.32 |
| | 426 | 2451 | 339 | 116.56 | 7.26 | 263.70 | 2.61 | 0.16 | 0.19 |
| | 421 | 1703 | 320 | 104.72 | 4.26 | 286.90 | 5.47 | 0.33 | 0.26 |
| | 334 | 1847 | 273 | 106.00 | 18.54 | 210.09 | 2.23 | 0.10 | 0.34 |
| | 347 | 5874 | 724 | 155.37 | 38.15 | 337.76 | 9.57 | 0.14 | 0.25 |
| | 325 | 5502 | 714 | 152.32 | 9.28 | 327.38 | 5.98 | 0.22 | 0.17 |
| | 312 | 1876 | 275 | 106.89 | 13.97 | 239.87 | 2.63 | 0.14 | 0.22 |
| S5 | 596 | 4036 | 538 | 137.51 | 22.34 | 297.28 | 6.49 | 0.19 | 0.37 |
| | 538 | 4629 | 591 | 143.66 | 17.70 | 241.27 | 3.45 | 0.23 | 0.43 |
| | 538b | 4520 | 577 | 142.55 | 720.66 | 247.62 | 2.43 | 0.14 | 0.26 |
| | 536 | 5037 | 640 | 147.75 | 14.53 | 328.11 | 7.38 | 0.24 | 0.33 |
| | 456 | 6326 | 933 | 160.41 | 17.73 | 327.90 | 9.25 | 0.25 | 0.29 |
| | 426 | 2446 | 344 | 116.59 | 11.46 | 259.62 | 2.85 | 0.24 | 0.25 |
| | 421 | 1842 | 271 | 106.29 | 22.11 | 206.27 | 1.95 | 0.11 | 0.28 |
| | 334 | 1842 | 271 | 106.29 | 22.11 | 206.27 | 1.95 | 0.11 | 0.28 |
| | 347 | 5771 | 723 | 154.48 | 13.65 | 309.75 | 6.35 | 0.30 | 0.37 |
| | 347b | 5722 | 727 | 154.20 | 9.71 | 252.06 | 2.71 | 0.21 | 0.27 |
| | 325 | 5421 | 702 | 151.54 | 8.61 | 334.18 | 6.43 | 0.27 | 0.26 |
| S6 | 665 | 4552 | 626 | 143.30 | 7.54 | 287.46 | 3.44 | 0.20 | 0.21 |
| | 565 | 4408 | 626 | 141.97 | 4.03 | 151.72 | 0.64 | 0.15 | 0.23 |
| | 546 | 6452 | 895 | 161.04 | 6.14 | 357.70 | 6.86 | 0.22 | 0.19 |
| | 354 | 7421 | 961 | 168.28 | 4.28 | 349.50 | 5.71 | 0.19 | 0.20 |
| | 354b | 2703 | 398 | 120.59 | 15.06 | 236.34 | 3.16 | 0.27 | 0.26 |
| | 235 | 3542 | 529 | 132.27 | 11.10 | 310.54 | 6.03 | 0.34 | 0.27 |

**Table 3** – *continued*

| S | GLO | $N_{\rm dark}$ | $N_{\rm bar}$ | $V_{\rm vir}$ | $R_{\rm opt}$ | $V_{\rm opt}$ | $M_{\rm star}$ | $Z_{\rm gas}/Z_\odot$ | $Z_{\rm star}/Z_\odot$ |
|---|---|---|---|---|---|---|---|---|---|
| | 234 | 1994 | 275 | 108.84 | 17.48 | 212.84 | 1.94 | 0.16 | 0.21 |
| | 235b | 4213 | 612 | 139.89 | 20.71 | 279.96 | 5.41 | 0.23 | 0.32 |
| | 127 | 6892 | 797 | 163.51 | 21.66 | 329.06 | 7.08 | 0.21 | 0.28 |
| S7 | 554 | 2748 | 385 | 121.21 | 8.98 | 268.50 | 3.60 | 0.28 | 0.27 |
| | 412 | 2583 | 340 | 118.32 | 5.26 | 231.50 | 2.00 | 0.22 | 0.29 |
| | 411 | 2214 | 338 | 113.20 | 3.81 | 145.39 | 0.92 | 0.25 | 0.31 |
| | 412b | 4954 | 640 | 147.00 | 10.93 | 314.43 | 5.44 | 0.37 | 0.25 |
| | 344 | 2673 | 317 | 119.35 | 5.93 | 282.17 | 4.44 | 0.49 | 0.34 |
| | 261 | 2839 | 362 | 122.09 | 7.49 | 287.67 | 4.79 | 0.39 | 0.27 |
| | 215 | 3951 | 518 | 136.39 | 11.32 | 260.92 | 3.10 | 0.27 | 0.21 |
| | 215b | 3884 | 510 | 135.67 | 18.21 | 223.06 | 1.57 | 0.16 | 0.19 |
| | 275 | 10743 | 1417 | 190.48 | 14.20 | 382.86 | 13.14 | 0.27 | 0.28 |
| | 232 | 8844 | 1204 | 178.73 | 5.95 | 403.29 | 7.78 | 0.16 | 0.18 |
| | 235 | 2162 | 244 | 110.95 | 3.50 | 195.64 | 1.93 | 0.42 | 0.25 |
| | 233 | 4002 | 574 | 137.52 | 10.37 | 257.12 | 3.73 | 0.30 | 0.31 |
| | 245 | 2206 | 258 | 111.88 | 8.03 | 250.97 | 2.97 | 0.30 | 0.30 |
| | 222 | 3148 | 412 | 126.46 | 8.00 | 286.05 | 5.11 | 0.36 | 0.30 |
| | 225 | 2474 | 370 | 117.37 | 13.47 | 258.48 | 3.98 | 0.26 | 0.22 |
| | 131 | 2292 | 244 | 112.97 | 18.75 | 191.21 | 0.57 | 0.09 | 0.11 |
| | 131b | 2335 | 244 | 113.59 | 31.22 | 220.19 | 1.52 | 0.17 | 0.21 |
| | 134 | 6934 | 981 | 165.10 | 11.23 | 365.57 | 8.53 | 0.22 | 0.25 |
| | 135 | 9700 | 1311 | 184.27 | 10.60 | 364.38 | 6.89 | 0.17 | 0.19 |

$[V] = {\rm km\,s^{-1}}$; $[M_{\rm star}] = 10^{10}\,{\rm M}_\odot$, $[R_{\rm opt}] = {\rm kpc}$.

### 4.1 Numerical experiments

We performed SPH simulations consistent with a cold dark matter (CDM) spectrum with $\Omega = 1$, $\Lambda = 0$, $\Omega_{\rm b} = 0.1$ and $\sigma_8 = 0.67$. We used $N = 262\,144$ particles ($M_{\rm part} = 2.6 \times 10^8\,{\rm M}_\odot$) in a comoving box of length $L = 5\,h^{-1}\,{\rm Mpc}$ ($H_0 = 100\,h^{-1}\,{\rm km\,s^{-1}\,Mpc^{-1}}$, $h = 0.5$), starting at $z = 11$. Note that dark matter and baryonic particles have the same mass. The gravitational softening used in these simulations is 3 kpc, and the smaller smoothing length allowed is 1.5 kpc. Simulations S1 to S5 share the same initial conditions, while S6 shares the SF and SN model parameters of S2, but has different random phases.

Simulations include SF and metallicity effects as described in Section 2. According to the discussion carried out in the previous section, the values of $C$, $\Theta_{\rm SN}$ and $t_{\rm SNI}$ affect the chemical composition of the stellar and gaseous components. In order to assess the impact of these parameters on the chemical properties of galactic objects, we have performed simulations with the same initial condition but varying the model parameters (see Table 2). We also compare results from simulations where the two adopted yields, PCB98 and WW95, have been used. We will focus on the study of global chemical properties of the ISM and the stellar populations of GLOs, and their relation with the dynamical parameters of the objects.

In order to study the properties of GLOs at $z = 0$, we identify them at their virial radius ($\delta\rho/\rho \approx 200$; White & Frenk 1991). In Table 3 we give their total dark matter ($N_{\rm dark}$) and baryonic ($N_{\rm bar}$) particle numbers within the virial radius and their virial circular velocity ($V_{\rm vir}$). Letter 'b' in the label code of the GLO (second column, Table 3) indicates that the main baryonic system is formed by a pair of galactic objects. From the set of GLOs identified, we are only going to analyse those with more than 250 baryonic particles within their virial radius.

As is well known, GLOs are formed by a dark matter halo that generally hosts a main baryonic clump and a series of satellites. All quantities measured at the virial radius are related to these complex systems. However, if we want to confront the simulated results with observations, it has to be taken into account that observed astrophysical quantities come from the luminous matter. For this purpose, we define a galactic object (GAL) as the structure determined by the main baryonic clump (including the dark matter mixed within it) hosted by a GLO.

The radius that encloses 83 per cent of the luminous mass of an exponential disc corresponds to the isophote of 25 mag arcsec$^{-2}$. Assuming the mass-to-luminosity ratio to be independent of radius, we define the optical radius of a GAL as the one that encloses 83 per cent of its baryonic mass. All chemical and astrophysical properties will be referred to twice the optical radius ($2R_{\rm opt}$), unless otherwise stated (see Table 3). This definition allows us to carry out a more meaningful comparison with observations. In this respect, $V_{\rm opt}$, defined as the circular velocity at $2R_{\rm opt}$, is determined by the baryonic and dark matter distributions in GALs, and consequently it is related to the physical mechanisms responsible for the concentration and distribution of the matter in the central region of a GLO (i.e. star formation, mergers, gas inflows, environment). Conversely, $V_{\rm vir}$ is a global parameter determined by the total potential well of the system.

Recall that, in these simulations, there are three types of baryonic particles: pure gaseous, hybrid and total stellar ones. We identify those that belong to a given GLO and its GAL, and look at their chemical properties within $2R_{\rm opt}$ at $z = 0$.

### 4.2 Global chemical properties

In this section we study the correlations between chemical and dynamical properties of the GALs, in order to explore the possible physical mechanisms that may determine the metallicity of a galaxy, and to assess the dependence on model parameters.

Observationally, defining the metallicity of a galaxy is a complex matter, since it depends on the type and quality of available data, the element used as the estimator, etc. (e.g. Kunth & Ostlin 1999). Moreover, observations only give information on

the metallicity of certain regions within a galaxy, so that they could be considered good estimators of the global metallicity only if the ISM were efficiently mixed.

Let us first review the main hypotheses of the one-zone simple model in order to understand the differences and advantages of our chemical scheme. The two basic assumptions of the simple model are: (a) the system is isolated and (b) it is well mixed at all times. Instantaneous recycling is also generally assumed.

Concerning hypothesis (a), our galactic objects form consistently with a hierarchical clustering scenario via the aggregation of substructure. At $z = 0$ a galactic object generally consists of a dark matter halo, a main baryonic clump and a series of satellites. Even if the objects do not have nearby similar-mass objects, they are rarely isolated. Moreover, there are always both gas infall from the dark matter haloes and encounters with satellites that may tidally induce gas inflows as have been reported in numerical (e.g. Mihos & Hernquist 1996; Tissera 2000) and observational works (Barton, Geller & Kenyon 1999). At higher $z$, interactions and mergers notably increase so that the hypothesis of a 'closed box' is never valid since what is observationally identified as a galaxy is just a component of the whole system. It has also to be stressed that the star formation history is affected by the evolution of the galactic object. This evolutionary process determines the different chemical properties of the objects in our simulations (for details see Paper II).

Owing to the mixing mechanism adopted, which depends on the local gas density, and the fact that the systems are never isolated, the metallicity of the gas and the new-born stellar population is not uniform. At a given time, we found a significant spread in the values of the ISM metallicities within a given GAL (Paper II). These results are consistent with those from chemodynamical models (e.g. Samland et al. 1997). Regarding instantaneous recycling, we follow the evolution of the populations according to the stellar masses including Type I and Type II supernovae explosions. A consistent implementation of SNI is performed as described in Section 2.2. Planetary nebulae (PNe) have not been included in this work.

Unfortunately we cannot treat the ISM in as much detail as chemodynamical models do, but this drawback is compensated by the fact that galaxy formation is well described according to a cosmological framework without ad hoc hypotheses. Moreover, the coupled non-linear evolution of dark matter and baryons has non-negligible effects on the star formation (e.g. Navarro & Steinmetz 2000; Paper II) which is directly related to the enrichment process.

We will first attempt to assess which dynamical parameters correlate with the chemical properties of the GALs. We define global quantities for the chemical content of GALs. A global metallicity ($Z$) is assigned to the stellar population and to the gaseous component of a GAL, taking into account all contributions from either the stars or the gas, respectively, according to

$$Z_a = \frac{\sum_{k=1}^{n} M_k}{M_a}, \tag{4}$$

where $a$ refers to the component (i.e. stars or gas), $M_k$ is the total mass of chemical element $k$ present in the $a$ component, $n$ is the total number of chemical elements $k$ considered, and $M_a$ is the total mass of the $a$ component within twice the optical radius. The estimated $Z_{\rm star}$ and $Z_{\rm gas}$ for each GAL are listed in Table 3.

We have analysed the GALs formed in simulations S2, S6 and

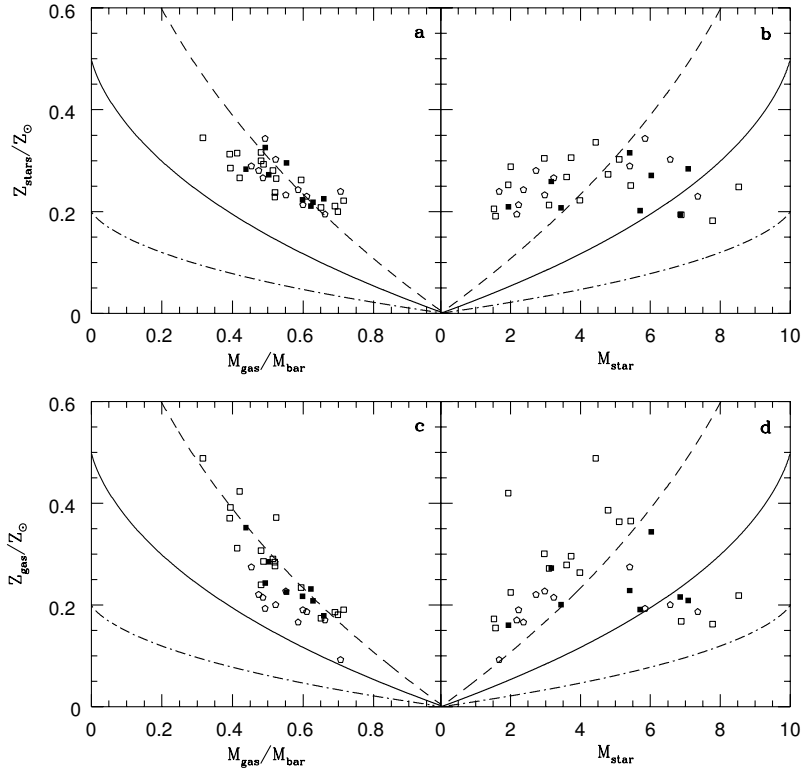


**Figure 5.** Global metallicities of the stellar population and gas component in GALs as a function of (a,c) their gas fraction, $M_{\rm gas}/M_{\rm bar}$, and (b,d) their total stellar mass, $M_{\rm star}$, in simulations S2 (open pentagons), S6 (filled squares) and S7 (open squares). Lines represent the relations given by the simple model for $0.2\,Z_\odot$ (dotted-dashed lines), $0.5\,Z_\odot$ (solid lines) and $1.0\,Z_\odot$ (dashed lines). $M_{\rm star}$ is given in units of $10^{10}\,M_\odot$.

S7. These experiments have the same star formation and cosmological model parameters but different random phases in the initial conditions. The SN parameters used in these experiments are taken from the best results given by the test runs ($t_{\rm SNI} = 10^8$ yr, $\Theta_{\rm SN} = 2$). In Figs 5(a) and (c) we show the global metallicities of the stellar population ($Z_{\rm star}$) and the gaseous component ($Z_{\rm gas}$) of the GALs versus their gas fractions. We find the expected trend indicating that the smaller the left-over gas, the higher the metallicity. Note that the slopes of this relation for the gas and the stars are different, being steeper for the former. The averaged values of global metallicities for these runs are: $\langle Z_{\rm star}/{\rm Z}_\odot\rangle = 0.25 \pm 0.05$ and $\langle Z_{\rm gas}/{\rm Z}_\odot\rangle = 0.24 \pm 0.09$. Note that we are considering the metal content of stars and gas particles within $2R_{\rm opt}$ irrespective of their particular location. These mean metallicity values cannot be directly compared to that of disc stars in the solar neighbourhood.

In Figs 5(b) and (d), we plot $Z_{\rm star}$ and $Z_{\rm gas}$ versus the total stellar mass ($M_{\rm star}$) within $2R_{\rm opt}$. As can be seen there is no clear trend between these parameters, albeit a weak tendency to have the higher metallicities in both gaseous and stellar components of GALs with intermediate stellar masses: $3\text{–}6 \times 10^{10}\,{\rm M}_\odot$.

For comparison, we have estimated these relations for our GALs assuming they have behaved according to the simple model. We include three cases: $0.2\,{\rm Z}_\odot$ (dotted-dashed lines), $0.5\,{\rm Z}_\odot$ (solid lines) and $1.0\,{\rm Z}_\odot$ (dashed lines). [In Figs 5(b) and (d), lines represent the estimations of the simple model for a system with total mass $M_{\rm bar} = 10^{10}\,{\rm M}_\odot$, initially with $M_{\rm star} = 0$ and $Z = 0$.] The significant differences between the simple model and the results of the numerical simulations can be appreciated. The slope of $Z_{\rm star}/{\rm Z}_\odot$ versus $M_{\rm gas}/M_{\rm bar}$ is different, as well as the systematic increase of stellar metallicity as a function of the stellar mass formed in the simple model, which contrasts with the behaviour of the numerical simulations. By inspection of the same relation for the gaseous components, we find that the simple model overestimates the metallicity of the galactic gaseous components for the parameters that match the chemical distribution of the stars. Hence, it seems that it is not possible to reproduce simultaneously the trends found in the stellar population and the gas of the simulated GALs with the simple model. This is somewhat expected since our code takes into account more complex processes (such as mergers, interactions, gas infall, etc.) that are not considered in the simple model.

We have studied the dependence of $Z_{\rm star}$ on $V_{\rm vir}$ and $V_{\rm opt}$, finding no significant correlations. We expected the lack of correlation with $V_{\rm vir}$ since it is determined by the whole gravitational bound system, while the chemical properties of the GALs are more strongly related to the fate of the baryonic matter in the internal regions. In fact, Fig. 6(a) shows no significant trend between the stellar mass of the GALs and their virial velocity. On the contrary, there is a clear correlation of $M_{\rm star}$ with $V_{\rm opt}$ as can be seen from Fig. 6(b). If a universal value for the stellar mass-to-light ratio is assumed, this correlation would imply a Tully–Fisher relation similar to those found in previous works (e.g. Tissera et al. 1997; Navarro & Steinmetz 2000). Given that our GALs follow the Tully–Fisher relation, one would expect, in principle, a correlation of the stellar population metallicity with the $V_{\rm opt}$, which is not found. We think that this lack of correlation is due to the fact that the chemical properties of these GALs are also affected by their merger history. Violent events have a strong impact on the baryon distributions and, consequently, on the mixing of metals (White 1981; Cora et al. 2001). Furthermore, these objects are continuously accreting gas, which contributes with pristine material to form new stars. From these results we find that the mean metallicity of the stellar population of the GALs cannot be directly linked to the optical mass either. Note that the lack of SN wind effects in our simulations, as first discussed by Dekel & Silk (1986), could strongly affect the evolution of the gaseous component of low virial mass haloes, producing a non-negligible effect on the chemical properties of these systems.

We have also studied how the properties discussed above change for different nucleosynthesis yield models. We have analysed the relations shown in Fig. 5 for experiment S1, which has been run with the same SF and SN parameters as used in S2, but with the nucleosynthesis model of PCB98 instead of that of WW95. In Fig. 7(a), a similar correlation can be seen as in Fig. 5(a), although with a shallower slope; and a lack of correlation between $Z_{\rm star}$ and $M_{\rm star}$ is apparent in Fig. 7(b). It can also be appreciated that global metallicities in the simulation with the PCB98 model are higher than those in simulations using WW95 yields, with average values of $\langle Z_{\rm gas}/{\rm Z}_\odot\rangle = 0.40 \pm 0.11$ and$\langle Z_{\rm star}/{\rm Z}_\odot\rangle = 0.45 \pm 0.06$. Hence, the different yields used imply significantly different results.

In order to explore the effects of changing the model parameters, $\Theta_{\rm SN}$, $t_{\rm SNI}$ and $C$, in Fig. 8 we plot $Z_{\rm star}$ versus $M_{\rm gas}/M_{\rm bar}$ and $M_{\rm star}$ for simulations S3, S4 and S5 (see Table 2). By inspection of Fig. 8(a) we can see that this correlation is present for all these experiments except S3. This simulation has the most efficient star formation, the largest value of $C$, which is

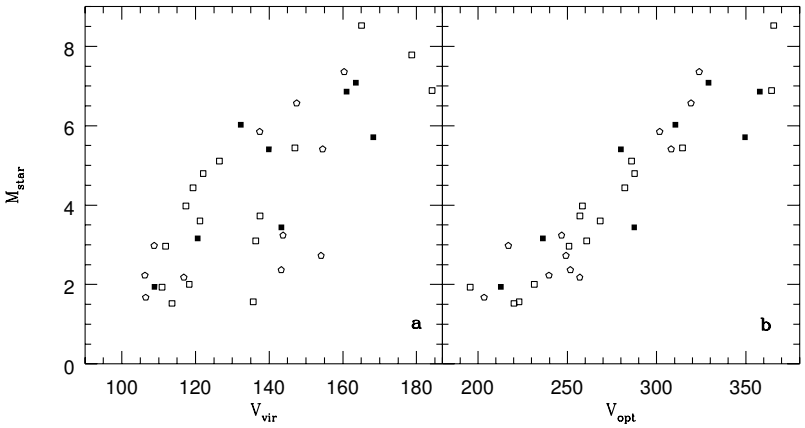


**Figure 6.** The total stellar mass of GALs ($M_{\rm star}$) as a function of (a) the virial velocity ($V_{\rm vir}$) and (b) the optical velocity ($V_{\rm opt}$) for the same GALs as shown in Fig. 5. Velocities are given in $\rm km\,s^{-1}$ and $M_{\rm star}$ is given in units of $10^{10}\,{\rm M}_\odot$.

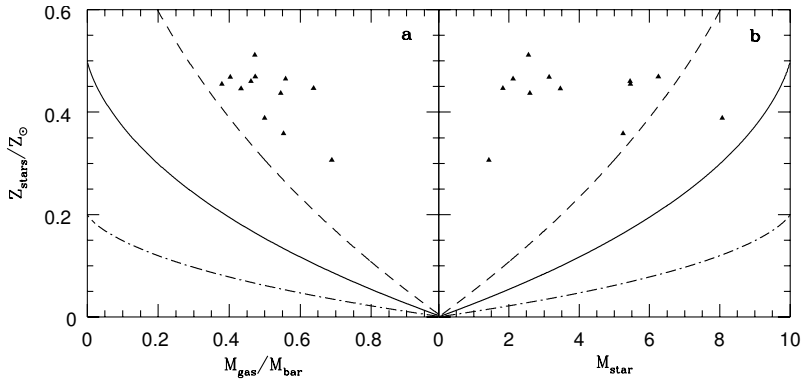


**Figure 7.** Global metallicities of the stellar populations in GALs ($Z_{star}/Z_{\odot}$) in simulation S1 (PCB98) as a function of (a) the gas fraction ($M_{gas}/M_{bar}$), and (b) the total stellar mass ($M_{star}$) of GALs. $M_{star}$ is given in units of $10^{10}M_{\odot}$. Lines represent the relations given by the simple model as in Fig. 5.

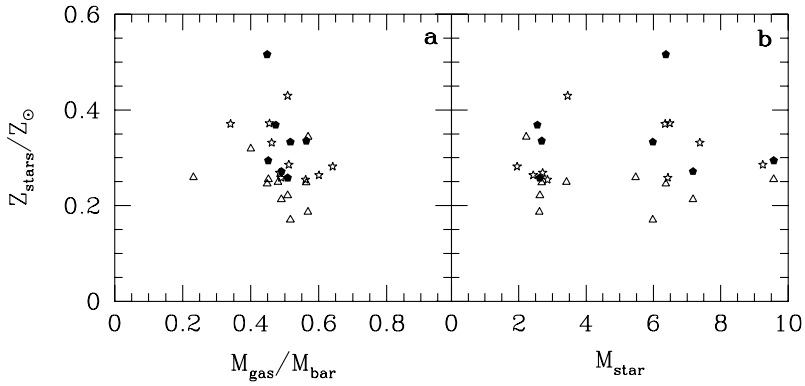


**Figure 8.** Global metallicities of the stellar populations ($Z_{star}/Z_{\odot}$) as a function of (a) the gas fraction ($M_{gas}/M_{bar}$), and (b) the total stellar mass ($M_{star}$) of GALs, in simulations S3 (filled pentagons), S4 (open triangles) and S5 (open stars). $M_{star}$ is given in units of $10^{10}M_{\odot}$.

**Table 4.** Mean $Z_{star}$ and $Z_{gas}$ values of GALs.

| | S1 | S2 | S3 | S4 | S5 | S6 | S7 |
|---|---|---|---|---|---|---|---|
| $\langle Z_{gas}/Z_{\odot}\rangle$ | $0.45 \pm 0.11$ | $0.21 \pm 0.06$ | $0.29 \pm 0.14$ | $0.18 \pm 0.06$ | $0.21 \pm 0.06$ | $0.22 \pm 0.06$ | $0.27 \pm 0.10$ |
| $\langle Z_{star}/Z_{\odot}\rangle$ | $0.43 \pm 0.06$ | $0.26 \pm 0.05$ | $0.44 \pm 0.15$ | $0.25 \pm 0.05$ | $0.31 \pm 0.06$ | $0.24 \pm 0.04$ | $0.26 \pm 0.06$ |

an important parameter that strongly affects star formation and metallicity: for higher $C$ values, and keeping the SN parameters fixed, the dispersion in metallicity increases. Note, however, that if the rate of SNI is decreased (larger $\Theta_{SN}$) and the $t_{SNI}$ is increased, this correlation is recovered (S4). Hence, these three parameters are relevant to determining the global chemical properties of the GALs. In the case of the relation between metallicity and luminosity (total stellar mass), the correlation is not present, as can be seen from Fig. 8(b). However, we cannot study the relative importance of the model parameters further unless we look in more detail at the chemical properties of the gaseous and stellar components (to be analysed in Paper II).

Estimates of the mean $Z_{star}$ and $Z_{gas}$ values of GALs in each simulation (see Table 4) show that, when the gaseous component is more gradually transformed into stars (S1, S2, S6, S7), the mean global metallicity of stellar populations and the ISMs at $z = 0$ are very similar, independent of the nucleosynthesis yield models used. Conversely, when the SF efficiency is increased (S3, S4, S5), the difference between the mean $Z_{star}$ and $Z_{gas}$ becomes very important. In this case, most of the metals are locked into stars, regardless of the SN parameters. Hence, in our chemical model a very efficient SF process produces, on average, ISMs considerably less metal-rich than the stellar populations of the GALs.

However, it has to be noted that the mixing mechanism plays a key role in determining this result. A different implementation could lead to a more efficient distribution of metals in a shorter time-scale, quickly enriching the ISMs. Nevertheless, the way chemical elements are mixed in the ISM is still a controversial question that remains to be resolved from a theoretical and observational point of view.

Unfortunately, we cannot directly compare these results with those derived from analytical or chemodynamical models since the latter focus on the study of the Galaxy and do not have a sample in which the dependences on the dynamical parameters of the galactic objects could be studied. Raiteri et al. (1996), although describing a similar chemical model to the one studied in this paper and using the SPH technique, do not consider different galactic haloes, so that we cannot compare our findings with their results.

### 4.3 Comparison with observations

Observations of galactic and extragalactic H II regions and OB associations provide information about the chemical properties of the forming stellar population and the ISM. These observations give relations for some primary elements such as S, Ne and C, and for the so-called secondary ones, like nitrogen, as a function of the O/H ratio. In this section, we resort to these observational results to assess the global chemical properties of the stellar populations and ISM of the simulated GALs.

Concerning the primary elements, Galactic and extragalactic H II regions show that the S/O and Ne/O ratios do not depend on O/H. However, the dispersion in these ratios is quite large (Pagel 1997). The simple model actually predicts a similar behaviour, since, in this scheme, the ratios between the primary elements are constant. However, this model fails to reproduce the observed correlation between C/O and O/H. A similar problem is detected for the observed N/O versus O/H, which exhibits a steeper correlation than that predicted by this model. Note that most observations are obtained from H II regions, which are assumed to be good tracers of the metallicity of the galactic ISM.

We analyse the ISMs in our GALs, which are determined by the gas particle properties within $2R_{\rm opt}$. The global metallicity, $Z^k_{\rm gas}$, for each chemical element $k$ in the ISM of a GAL is defined as

$$Z^k_{\rm gas} = \frac{\sum_{i=1}^{n_{\rm p}} m_i^k}{M_{\rm gas}}, \qquad (5)$$

where $n_{\rm p}$ is the total number of $i$ gas particles within $2R_{\rm opt}$, $m_i^k$ is the mass of the $k$th element in the $i$th particle and $M_{\rm gas}$ is the total gas mass within $2R_{\rm opt}$. An equivalent relation can be defined for the stellar population, $Z^k_{\rm star}$.

In Fig. 9, we plot log(S/O) for the ISM in the GALs in simulations S2, S3, S4 and S5. As can be seen, the mean values obtained in the simulations are in very good agreement with observations (taken from Pagel 1997). The average log(S/O) for GALs shows a large dispersion that compares well with the observed values. The larger S/O ratios are obtained for the simulation with the highest SF efficiency (simulation S3). However, by changing SN parameters in order to diminish the effects of SNI explosions, and maintaining the same SF parameter in the simulation (simulation S4), we obtain substantially smaller abundance ratios and dispersions.

In Fig. 10, we plot log(C/O) versus log(O/H) for GALs in simulations S2, S3, S4 and S5 (WW95) and simulation S1 (PCB98). We include observations of H II regions (Pagel 1997). A remarkable fact that can be seen from this figure is the large difference between the results of the WW95 and PCB98 models. GALs in S1, which are exactly equivalent to those in S2, except for the nucleosynthesis model adopted, have ratios almost half an order of magnitude larger than their WW95 counterparts, and are beyond the observational range. Conversely, GALs in any of the WW95 runs have ISMs with abundances similar to the observed ones. However, they do not show the gradient reported from observations of Galactic and extragalactic H II regions (e.g. Garnett et al. 1995; Kennicutt & Garnett 1996; Kobulnicky & Skillman 1996), although the simulated abundances extend only in the range $-3.8 < \log({\rm O/H}) < -3.2$. The simulated mean values are lower than the observed ones but it has to be recalled that we are not including PNe yields that are thought to be important contributors of C (and N).

Observations of N/O in H II regions show that this ratio increases with O/H (e.g. Pagel 1992). A gradient in the secondary element is actually predicted by the simple model, although the

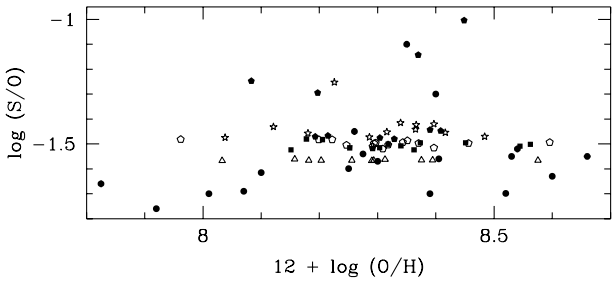


**Figure 9.** S/O versus O/H for the ISM of GALs in simulations S2, S3, S4 and S5 (see Figs 5 and 8 for feature code). Observations of H II regions have been included (filled circles).

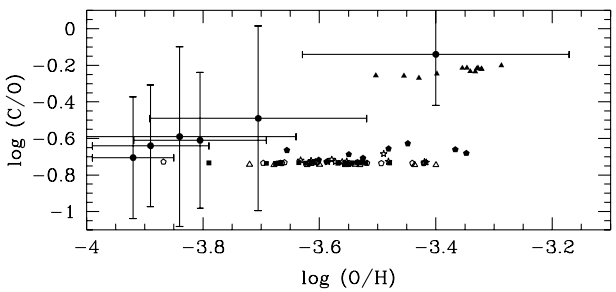


**Figure 10.** C/O versus O/H for the ISM of GALs in simulations S2, S3, S4 and S5 (see Figs 5 and 8 for feature code). GALs in S1 (filled triangles) have been included. Observations of H II regions have been included (filled circles).

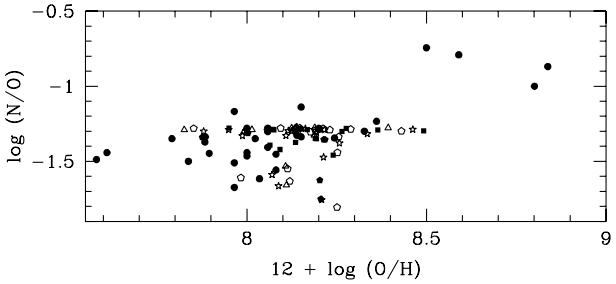


**Figure 11.** N/O versus O/H for the ISM of the GALs shown in Fig. 9. Observations of H II regions have been included (filled circles).

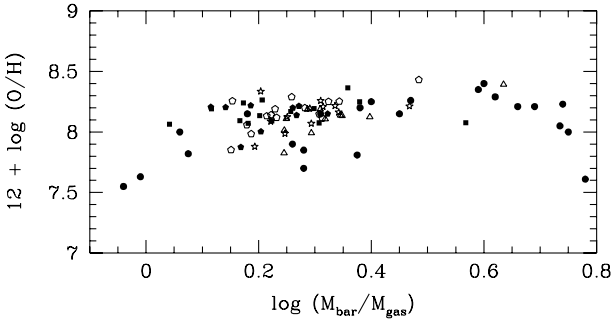


**Figure 12.** Logarithm of the oxygen abundances versus the logarithm of their gas fraction for the same GALs as shown in Fig. 9. Observations of H II regions in blue compact and irregular galaxies from Pagel (1997) have been included (filled circles).

steepness of the predicted relation is much larger than that actually observed in H II regions. There are several hypotheses that may explain the origin of these differences (Pagel 1997). We estimate this relation for GALs in WW95 runs. As shown in Fig. 11, the simulated ISMs have abundances that are in good agreement with observations. However, we only find GALs with $12 + \log(\mathrm{O/H}) < 8.5$, while the observed gradient in H II regions is $12 + \log(\mathrm{O/H}) > 8.5$. We find neither GALs with average ISM metallicity corresponding to solar abundances, nor extremely low-metallicity IZW18-type objects. It should be considered, however, that only massive GALs are analysed in the simulations.

Another important observational correlation is that between $12 + \log(\mathrm{O/H})$ and the gas fraction estimated for irregular and blue compact galaxies (e.g. Axon et al. 1988). This relation can be used to assess the metal content of the ISMs in relation to the left-over gas mass of the corresponding GALs. In Fig. 12, we plot $12 + \log(\mathrm{O/H})$ versus $\log(M_{\rm bar}/M_{\rm gas})$ for the ISM in the simulated GALs ($M_{\rm bar}$ and $M_{\rm gas}$ are the total baryonic and gaseous mass within $2R_{\rm opt}$, respectively). Observations taken from Pagel (1997) have been included for comparison. The estimated abundance ratios in the models are consistent with observations. It is notable that the observed relation is well reproduced, in the sense that objects with a lower gas fraction tend to have larger metallicities without the need to introduce other physical mechanisms, such as SN energy injection effects, into the ISM. The simple model predicts a decrease of the metallicity with the gas richness of the system, but it fails to reproduce correctly the observational relation.

## 5 CONCLUSIONS

We have implemented a chemical model in an SPH cosmological code. First results are reported together with the assessment of the effects of model parameters and numerical resolution. It is found that the major problem introduced by low numerical resolution is the artificial smoothing of the chemical properties of the objects. However, if a minimum number of baryonic particles is imposed, then average values can be considered reliable.

The mean metallicity is found to be nearly independent of the total stellar mass of the system, indicating that the effects of mergers, interactions and gas infall on the mass distribution and metal mixing are very significant. We find correlations between the stellar mass $M_{\rm star}$ and the virial and optical circular velocities ($V_{\rm vir}$, $V_{\rm opt}$). However, the correlation with $V_{\rm opt}$ is significantly tighter, consistent with the Tully–Fisher relation. Nevertheless, the global metallicity of GALs, $Z_{\rm star}$, shows no dependence on $V_{\rm opt}$, in spite of the fact that these GALs satisfy the Tully–Fisher relation, and shows a strong correlation between the global metallicity of their stars and gas components with the left-over gas fraction of the systems. We only find a significant correlation between the global GALs metallicity of both stars and gas with the left-over gas fraction of the systems.

An analysis of the GALs assuming they have behaved according to the one-zone simple model shows important differences with the results of the numerical simulations. The slope of $Z_{\rm star}/\mathrm{Z}_{\odot}$ versus $M_{\rm gas}/M_{\rm bar}$ and the systematic increase of stellar metallicity as a function of the stellar mass formed in the simple model contrasts with the behaviour of the numerical simulations. We find that the simple model overestimates the metallicity of the galactic gaseous components if it is constrained to match the stellar chemical content. According to the simple model, the global metallicity of a system continuously increases with the stellar mass, in disagreement with the results found for the simulated GALs, which show higher metallicities for intermediate-mass objects.

We find that the star formation efficiency, SN model parameters and the nucleosynthesis yields significantly affect the chemical properties of the GALs. In those models where the SF process is gradual, the mean stellar and gaseous metallicities are similar.

The observed abundance ratios for primary and secondary elements in Galactic and extragalactic H II regions are naturally obtained. However, the ranges of the simulated global metallicities are smaller than the observed ones. Also, the relation between the O/H ratio and gas fraction obtained in the numerical simulations is consistent with the observational results.

The suitable agreement between the models and the observations for these relations suggests that hierarchical clustering scenarios are able to reproduce the chemical properties of galaxies. This is a very encouraging fact taking into account that galactic objects form by the accretion and merger of substructures. Violent events are common and ubiquitous, and can affect the dynamical evolution of the matter, regulating the SF and chemical evolution in galactic objects.

We intend to improve this chemical model in the future by allowing the gaseous component to cool according to its metallicity, and by undertaking a further study of the mixing process of chemical elements in the ISM. Also under study is a more efficient decoupling mechanism between stars and gas, which could shorten the period of the hybrid state of a baryonic particle. Finally, energy feedback remains an open question that we hope to address in a future work.

## ACKNOWLEDGMENTS

We thank S. Woosley for kindly providing the yield tables, and L. Portinari for clarifying some aspects of their nucleosynthesis model. We acknowledge the careful reading of the manuscript by and useful suggestions of the anonymous referee. We also thank M. Abadi for useful discussions. P. Tissera is grateful to C. Chiappini for introductory discussion in chemical evolution during the 1999 Aspen Summer Workshop. The authors are grateful for the hospitality of the Observatorio Astronómico Centroamericano de Suyapa while finishing the writing of this paper. P. Tissera is grateful to the Observatorio Astronómico de Córdoba and the research group IATE for allowing the use of their computational facilities. M. Mosconi thanks IAFE for their hospitality during the preparation of this work. This work has been partially supported by CONICET, CONICOR, SECYT and Fundacion Antorchas.

## REFERENCES

Axon D. J., Staveley-Smith L., Fosbury R. A. E., Danziger J., Boksenberg A., Davies R. D., 1988, MNRAS, 231, 1077
Barnes J., Hernquist L., 1996, ApJ, 471, 115
Barton E., Geller M. J., Kenyon S. J., 2000, ApJ, 530, 600
Bottema A. H., 1992, A&A, 328, 517
Blumenthal G. R., Faber S. M., Flores R. A., Primack J. P., 1986, ApJ, 301, 27
Burkert A., Truran J. W., Hensler G., 1992, ApJ, 391, 651
Chiappini C., Matteucci F., Gratton R., 1997, ApJ, 477, 765
Cora S. A., Tissera P. B., Lambas D. G., Mosconi M. B., 2001, in Funes H. G., Corsini E. M., eds, ASP Conf. Ser. Vol. 230, Galaxy Disks and Disk Galaxies. Astron. Soc. Pac., San Francisco, p. 653
Courteau S., de Jong R. S., Broeils A. H., 1996, ApJ, 457, L73

Cowie L. L., Songaila A., Hu E. M., Cohen J. G., 1996, ApJ, 112, 839
Dalgarno A., McCray R. A., 1972, ARA&A, 10, 375
Dekel A., Silk J., 1986, ApJ, 303, 39
Domínguez-Tenreiro R., Tissera P., Sáiz A., 1998, ApJ, 508, L123
Edvardsson B., Andersen J., Gustafsson B., Lambert D. L., Nissen P. E., Tomkin J., 1993, A&AS, 274, 101
Ellis R. S., Colless M., Broadhurst T., Heyl J., Glazebrook K., 1996, MNRAS, 280, 235
Ferrini F., Matteucci F., Pardi C., Peuco U., 1992, ApJ, 387, 138
Garnett D. R., Sillman E. D., Dufour R. J., Peimbert M., Torres-Peimbert S., Shields G. A., Terlevich R. J., Terlevich E., 1995, ApJ, 443, 64
Gratton R., Cannetta E., Matteucci F., Sneden C., 1996, in Morrison H., Sanajedini A., eds, Formation of the Galactic Halo. Inside Out, Vol. 92
Greggio L., 1996, in Kunth D., Guiderdoni B., Heydari-Malayeri M., Thuan T., eds, The Interplay Between Massive Star Formation, the ISM and Galaxy Evolution. Editions Frontières, Gif-sur-Yvette, p. 89
Katz N., 1992, ApJ, 391, 502
Kennicutt R., Jr., Garnett D. R., 1996, ApJ, 456, 504
Kobulnicky H. A., Skillman E. D., 1996, ApJ, 471, 211
Kunth D., Ostlin G., 2000, ARA&A, 10, 1
Larson R., 1975, MNRAS, 173, 671
Larson R., 1976, MNRAS, 176, 31
Lilly S. J., Tiesse L., Hammer F., Crampton D., Le Fevre O., 1995, ApJ, 441, 18
Lu L., Sargent L. W., Barlow T., Churchill C., Vogt S., 1996, ApJS, 107, 475
Madau M. P., 1995, ApJ, 441, 18
Madau P., Ferguson H., Dickinson M., Giavalisco M., Steidel C., Fruchter A., 1996, MNRAS, 283, 1388
Matteucci F., Francois P., 1989, MNRAS, 239, 885
Metzler C. A., Evrard A. E., 1994, ApJ, 437, 564
Mihos J. C., Hernquist L., 1996, ApJ, 464, 641
Navarro J. F., Steinmetz M., 2000, ApJ, 538, 477
Navarro J. F., White S. D. M., 1994, MNRAS, 267, 401
Pagel B. E. J., 1992, in Alloin D., Stansiska G., eds, The Feedback of Chemical Evolution on the Stellar Content of Galaxies. Observatoire, Paris, p. 87
Pagel B. E. J., 1997, Nucleosynthesis and Chemical Evolution of Galaxies. Cambridge Univ. Press, Cambridge
Pettini M., Smith L., King D., Hunstead R., 1997, ApJ, 998, 665
Portinari L., Chiosi C., Bressan A., 1998, A&AS, 334, 505 (PCB98)
Raiteri C. M., Villata M., Navarro J. F., 1996, A&AS, 315, 105
Renzini A., 1998, in D'Odorico S., Fontana A., Giallongo E.,, eds, ASP Conf. Ser. Vol. 146, The Young Universe: Galaxy Formation and Evolution at Intermediate and High Redshift, Vol. 92. Astron. Soc. Pac., San Francisco, p. 298
Rhee M. H., 1996, PhD thesis, Univ. Groningen
Rocha-Pinto H. J., Maciel W. J., Flynn C., 2000, A&A, 358, 869
Samland M., Hensler G., Theis Ch., 1997, ApJ, 476, 544
Schmidt M., 1963, ApJ, 137, 758
Springel V., 2000, MNRAS, 312, 859
Steidel C. C., Hamilton D., 1992, AJ, 104, 941
Steidel C. C., Adelberger K. L., Giavalisco M., Dickinson M., Pettini M., 1998, ApJ, 519, 1
Steinmetz M., Müller E., 1994, A&A, 281, L97
Steinmetz M., Müller E., 1995, MNRAS, 276, 549
Tenorio-Tagle G., Sergey A. S., Kunth D., Terlevich E., Terlevich R., 1999, MNRAS, 309, 332
Thielemann F. K., Nomoto K., Hashimoto M., 1993, in Prantzos N., Vangoni-Flam E., Cassé N., eds, Origin and Evolution of the Elements. Cambridge Univ. Press, Cambridge, p. 299
Thomas P. A., Couchman H. M. P., 1992, MNRAS, 257, 11
Tinsley B. M., 1980, Fundam. Cosmic Phys., 5, 287
Tissera P. B., 2000, ApJ, 534, 636
Tissera P. B., Domínguez-Tenreiro R., 1998, MNRAS, 297, 177
Tissera P. B., Lambas D. G., Abadi M. G., 1997, MNRAS, 286, 384
Tosi M., 1996, in Leitherer C., Firtze-von Alvernsleben U., Huchra J., eds, ASP Conf. Ser. Vol. 198, From Stars to Galaxies: The Impact of Stellar Physics on Galaxy Evolution. Astron. Soc. Pac., San Francisco, p. 229
van den Bergh S., 1962, A&AS, 67, 486
van den Bergh S., 1991, ApJ, 369, 1
White S. D. M., 1981, MNRAS, 191, 1
White S. D. M., Frenk C. S., 1991, ApJ, 379, 25
Woosley S. E., Weaver T. A., 1995, ApJS, 101, 181 (WW95)

This paper has been typeset from a TEX/LATEX file prepared by the author.